

Design of a Reconfigurable Multi-Band Antenna with Partially Dredged Cloverleaf

Tao Tang^{1,*}, Jiawei Wang¹, Melad M. Olaimat², Tao Fang¹, and Xiexun Zhang¹

¹College of Electronic and Information, Southwest Minzu University, Chengdu, Sichuan 610225, China

²Department of Renewable Energy Engineering, Al Al-Bayt University, Mafraq, Jordan

ABSTRACT: This paper presents a novel reconfigurable multi-band antenna with a partially dredged cloverleaf shape that is tailored for size reduction and suitable for compact devices and urban environments. The antenna is capable of covering three distinct frequency bands: 3.22–4.06 GHz, 4.44–6.12 GHz, and 3.8–4.77 GHz, with respective bandwidths of 22%, 31.8%, and 22.6%, demonstrating its wideband capabilities. Utilizing various feeding configurations, the antenna enables the realization of multiple radiation patterns and frequency tuning. Validated through simulations and measurements, this design shows promise for 5G and advanced communication systems.

1. INTRODUCTION

Antennas play a crucial role in communication systems, as the need for improved data rates, efficient spectrum utilization, and reliable connectivity drives innovation in antenna design. Reconfigurable, broadband, and multi-band antennas are particularly noteworthy for meeting these demands, with a specific focus on miniaturization to accommodate compact devices and urban environments.

Reconfigurable antennas adapt to varying communication needs by adjusting parameters like frequency and radiation pattern [1]. They enhance system flexibility and capacity while simplifying design compared to multiple fixed antennas. Yet, bandwidth limitations, design intricacies, and efficiency losses during reconfiguration are challenges that require solutions [2].

Wideband antennas are ideal for applications needing extensive frequency ranges, offering ease of design and system compatibility [3]. While they may be larger and face impedance matching issues, their design allows for trade-offs between bandwidth and efficiency [4]. Multi-band antennas deliver the advantage of operating over several frequency bands, ensuring broad compatibility with various communication protocols [5]. However, they encounter challenges such as mutual coupling and sustaining consistent radiation patterns across different bands [6]. Innovations in miniaturization, such as metamaterials and fractal geometries, aim to meet the demands of modern devices, though there is a trade-off between size reduction and performance [7].

Deformable dipole antennas provide a dynamic response to changing conditions, offering broader bandwidth and efficiency for multi-system compatibility. Techniques like meandering and fractalization extend their operational capabilities [8], while specific configurations allow for precise control over radiation patterns [9]. The advent of 5G networks de-

mands ultra-high data rates and minimal latency, posing challenges in integrating small antennas and ensuring compatibility with existing systems [10].

This paper presents a novel reconfigurable, deformable dipole antenna designed for the 5G frequency band. Drawing inspiration from a cloverleaf shape with a partially reduced radiation element, the antenna achieves significant size reduction. It covers three key 5G bands: 3.22–4.06 GHz, 4.44–6.12 GHz, and 3.8–4.77 GHz, with bandwidths of 22%, 31.8%, and 22.6%, respectively, showcasing its wideband functionality. By employing various feeding configurations, the antenna supports multi-mode operation and adjustable radiation patterns, presenting an innovative solution that meets the compactness and performance demands of modern electronics.

2. CONFIGURATION AND RESULTS

Figure 1 shows a top view of the designed antenna, which consists of two pairs of antenna units operating at different frequencies, labeled A1 and A2, respectively, F4B-2 with a thickness of 0.508 mm and a relative permittivity of 2.65 served as the design basis for the antenna. The parameters of $L = 30.48$ mm, $W = 21.4$ mm, $L_1 = 14.24$ mm, $L_2 = 9.88$ mm, $L_3 = 7.48$ mm, $L_4 = 2.73$ mm, $W_1 = 10$ mm, $W_2 = 6.2$ mm, $W_3 = 8.4$ mm, and $W_4 = 5.8$ mm are respectively represented as the overall length and width of the antenna radiate, the length of the arms of the two deformed dipoles A1 and A2, the length of the cutoff part on the arms of A1 and A2, the width of the arms of A1 and A2, and the width of the cutoff part on the arms of A1 and A2.

As illustrated in Fig. 2, the proposed antenna demonstrates tri-mode functionality, operating across distinct frequency bands, and all operating bands have wideband characteristics. First, antennas A1 and A2 are configured to resonate at

* Corresponding author: Tao Tang (tangt@swun.edu.cn).

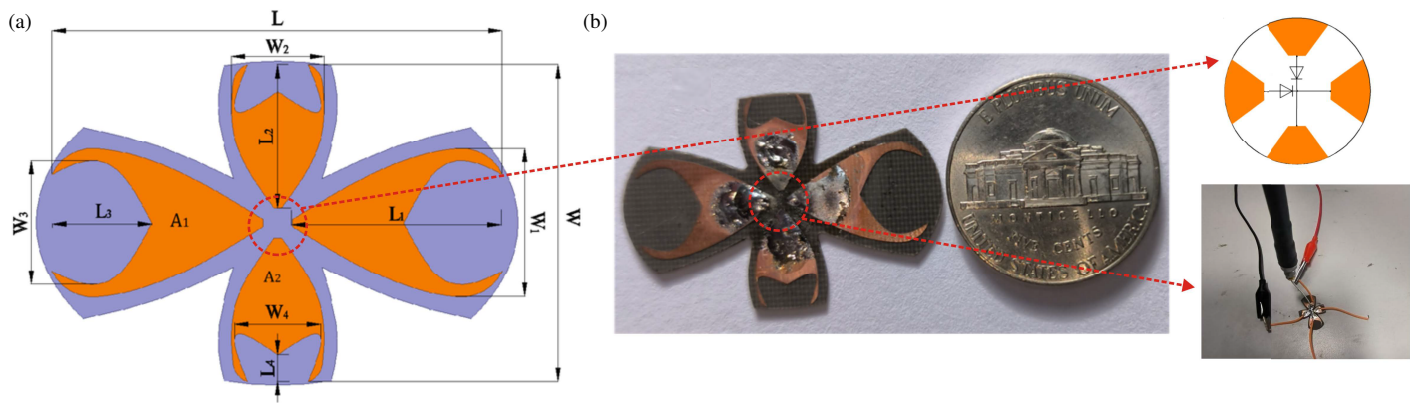


FIGURE 1. Configuration of the antenna. (a) Configuration, (b) prototype.

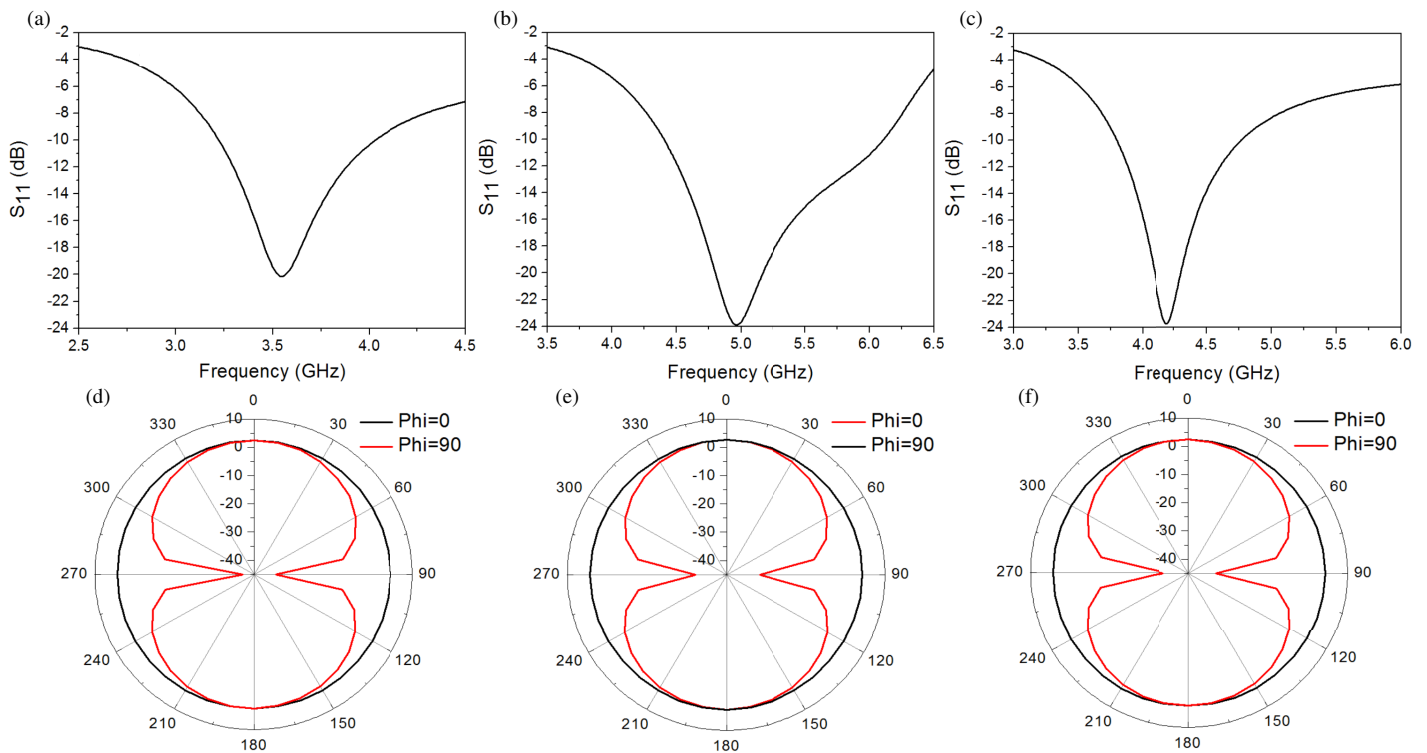


FIGURE 2. S_{11} and radiation patterns of the antenna. (a) S_{11} of A1, (b) S_{11} of A2, (c) S_{11} of the left arm of A1 and the upper arm of A2 are fed, (d) radiation pattern of A1 at 3.5 GHz, (e) radiation pattern of A2 at 4.9 GHz, (f) radiation pattern of the left arm of A1 and the upper arm of A2 are fed at 4.2 GHz.

frequencies of 3.5 GHz and 4.9 GHz with a bandwidth of 23% (3.22–4.06 GHz) and 31.8% (4.44–6.12 GHz), respectively, which align with the 5G frequency band. Additionally, when feeding one arm of A1 and one arm of A2 (for example, the left arm of A1 and the upper arm of A2 as shown in Fig. 1(a)), resonance is achieved at 4.2 GHz with a bandwidth of 22.6% (3.8–4.77 GHz). Figs. 2(a)–(c) display the S_{11} parameters for the different feeding configurations of A1 and A2, while Figs. 2(d)–(f) present the corresponding radiation patterns for each operational mode.

Utilizing one arm from each of the antennas A1 and A2 activates four distinct operational modes, as shown in Fig. 1(a): (1) the left arm of A1 with the upper arm of A2, (2) the right arm of A2 with the upper arm of A1, (3) the left arm of A1 with

the lower arm of A2, and (4) the right arm of A1 with the lower arm of A2. The corresponding radiation patterns for these four modes are illustrated in Fig. 3. It can be observed that the radiation remains consistent across all cases, with a slight leftward skew in cases (1) and (3) and a slight rightward skew in cases (2) and (4). However, these deviations are minimal, with all deflections falling within a 5-degree range. The S -parameters for these four modes are shown in Fig. 2(c).

3. DESIGN PROCESS AND MEASUREMENTS

The original structure of the antenna given in Fig. 1(a) is derived from a dipole. Take A1 as an example to explain its design process. Increasing the arm width of the printed dipole

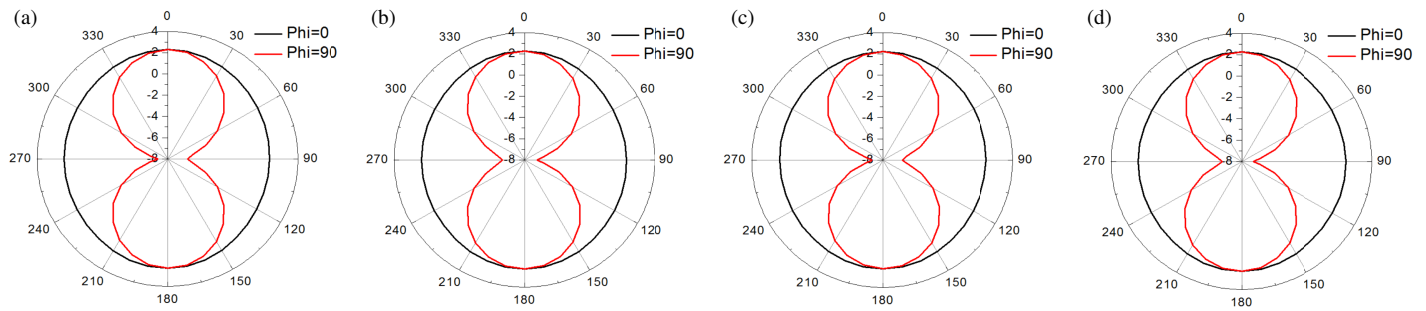


FIGURE 3. Radiation patterns of the antenna in different operation modes. (a) The left arm of A1 and the upper arm of A2, (b) the right arm of A2 and the upper arm of A1, (c) the left arm of A1 and the lower arm of A2, (d) the right arm of A1 and the lower arm of A2.

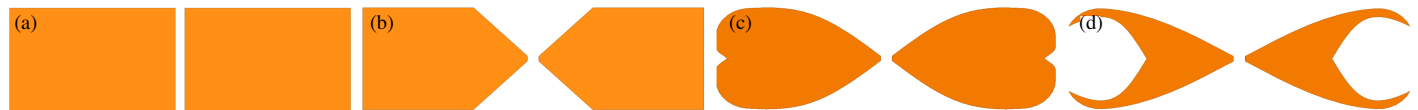


FIGURE 4. Evolution of the antenna. (a) Original structure, (b) flare angles cut, (c) cloverleaf, (d) partially dredged cloverleaf.

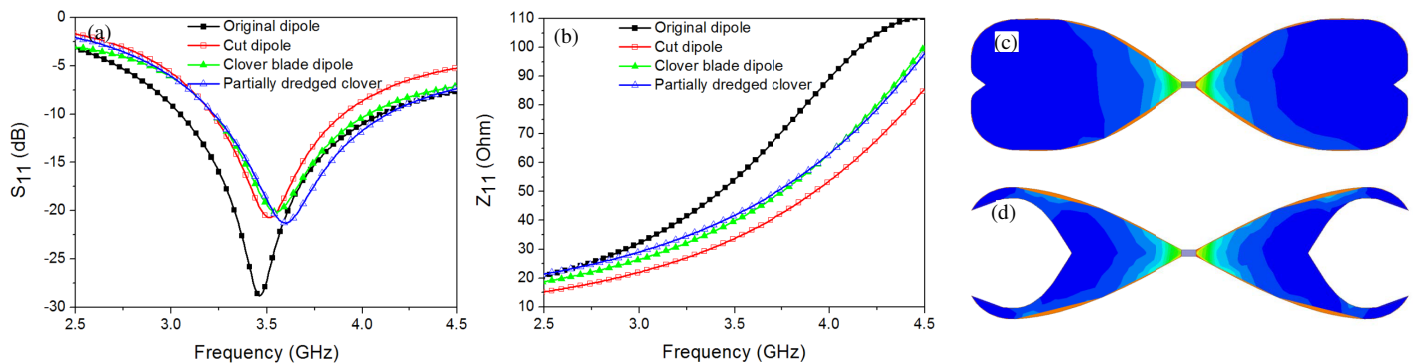


FIGURE 5. S_{11} and the input impedance as well as the surface current distribution on arms of the antenna with different shapes as shown in Fig. 4. (a) S_{11} , (b) impedance, (c) surface current of the cloverleaf, (d) surface current of the partially dredged cloverleaf.

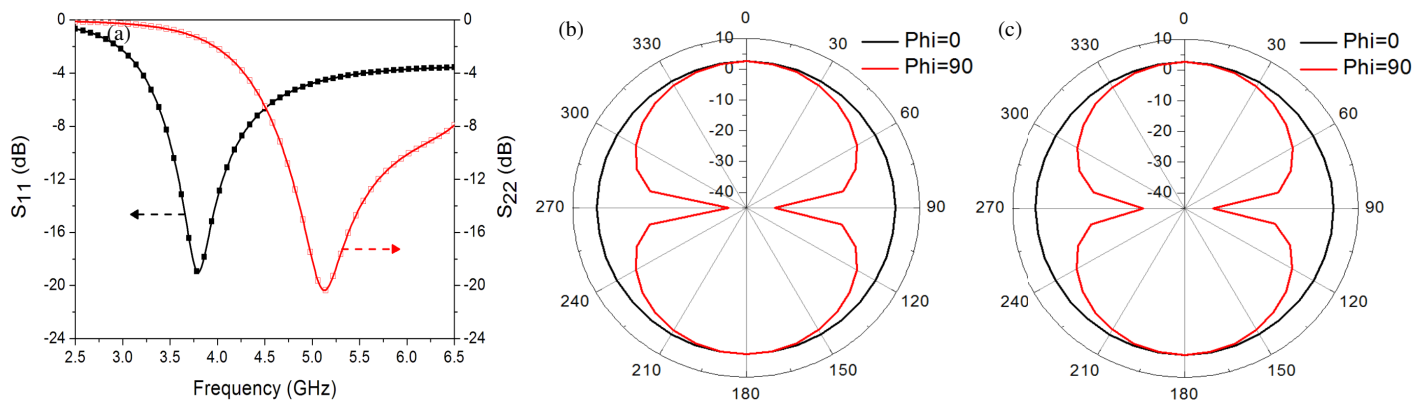


FIGURE 6. S -parameters and radiation patterns of A1 and A2 are fed simultaneously. (a) S -parameters, (b) radiation pattern of A1, (c) radiation pattern of A2.

antenna can effectively increase the operating frequency band of the dipole [11], so as shown in Fig. 4(a), two wide radiating arms are used to construct the dipole. To maintain a resonant frequency of 3.5 GHz, the overall size of the antenna is $36 \times 10 \text{ mm}^2$. The implementation of symmetrical flare angles at the feed points not only amplifies the dipole's bandwidth but

also provides key insights into optimizing dipole antenna performance [12]. Moreover, the strategic application of shear on the arm modifies the surface current path, allowing for a reduction in antenna length while preserving the resonant frequency, as shown in Fig. 4(b) where the length is adjusted to 30 mm. The cloverleaf-shaped arm, with a shear depth of 1 mm and

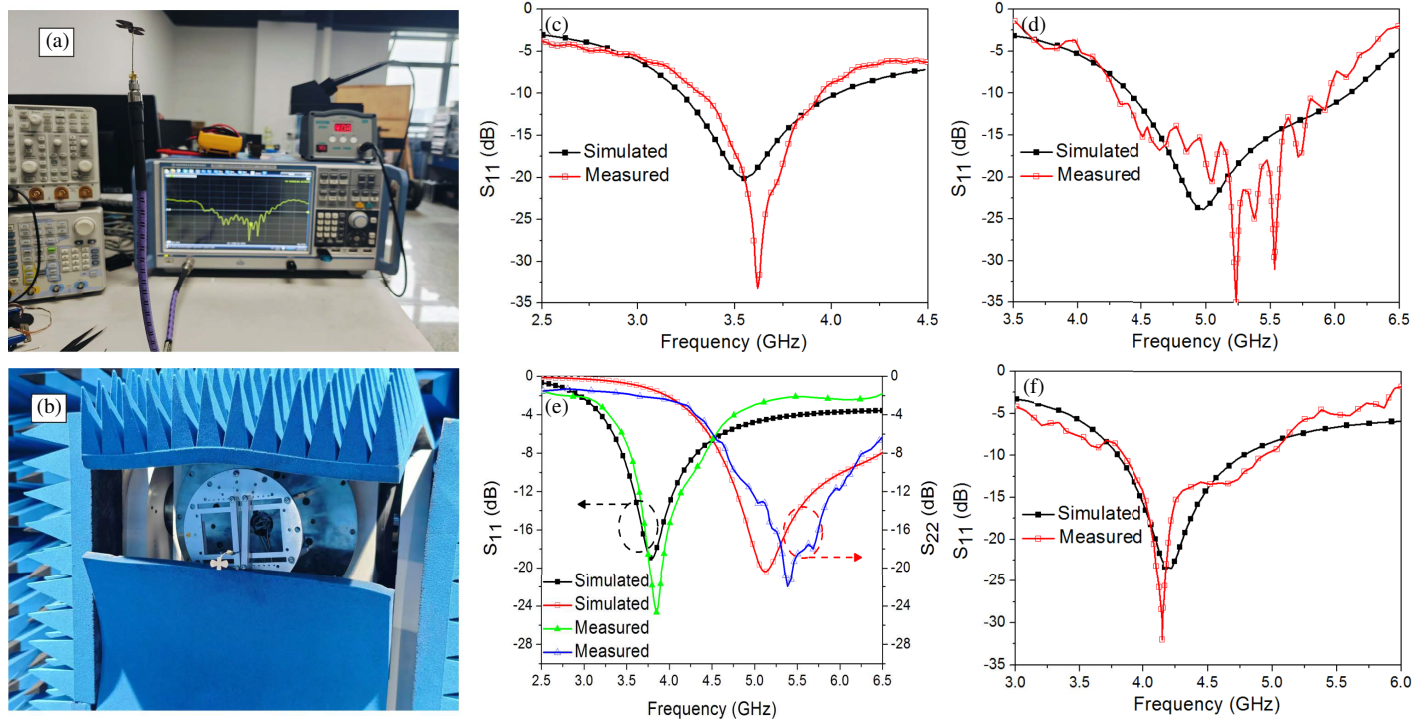


FIGURE 7. Measurement setup and measured S -parameters. (a) S -parameters measurement setup, (b) radiation measurement setup in the chamber, (c) mode 1, (d) mode 2, (e) mode 3, (f) one of the modes 4, 5, 6, and 7.

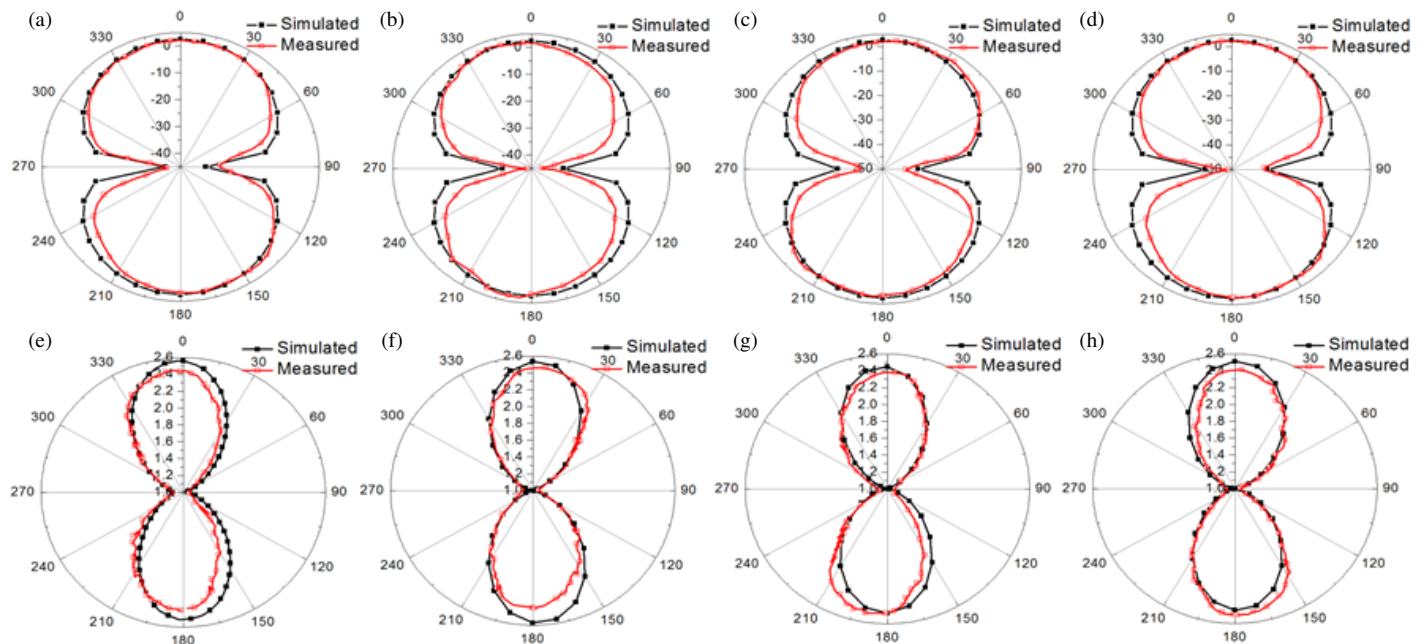


FIGURE 8. Measured radiation patterns. (a) Mode 1, (b) mode 2, (c) 3.8 GHz of mode 3, (d) 5.1 GHz of mode 3, (e) mode 4, (f) mode 5, (g) mode 6, (h) mode 7.


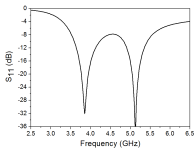
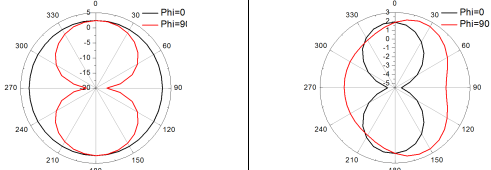
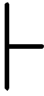
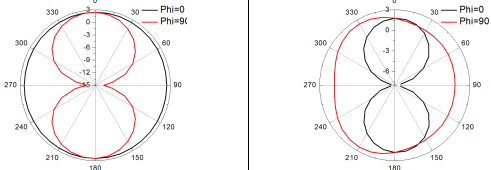

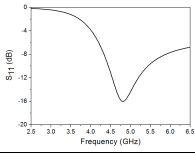
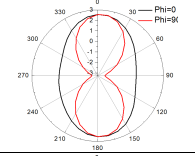
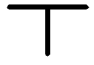
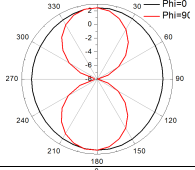
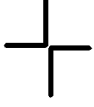
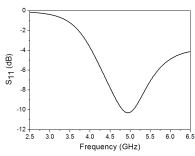
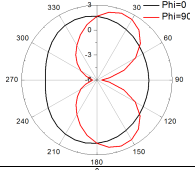
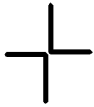
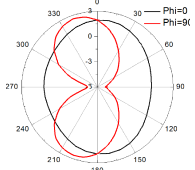
an angle of 73 degrees as indicated in Fig. 4(c), further refines impedance matching between the antenna arm and the port.

The S_{11} and input impedance of the antenna, as depicted in Fig. 4, are graphically represented in Fig. 5. It is observed from Fig. 5(a) that reducing the dipole arm length in three subsequent modifications causes an upward shift in the resonant frequency. Although this results in a slight decrease in bandwidth, the final

configuration has the widest working band. Fig. 5(b) illustrates that the three subsequent iterations have resulted in a more uniform input impedance profile of the antenna across the operation bandwidth.

The surface current on the antenna determines its radiation performance. As shown in Fig. 5(c), the surface current of the antenna (a) is concentrated near the feed source, so the part

TABLE 1. Simplified schematics of these six operational modes with corresponding S -parameters and radiation patterns.

Modes	Schematic diagram of antenna arm conduction form	S -parameters	Radiation patterns
8			
9		The same as Mode 8	
10			
11		The same as Mode 10	
12			
13		The same as Mode 12	

of the radiation arm with low current can be excavated to further reduce the antenna surface area. The final design shown in Fig. 4(d) is the shape of a partially dredged cloverleaf, and its corresponding surface current distribution is shown in Fig. 5(d).

If A1 and A2 are fed simultaneously, the antenna will exhibit different working frequency bands. Fig. 6 presents the S_{11} of A1, the S_{22} of A2, as well as their respective radiation patterns. As shown in Fig. 6, simultaneous operation of A1 and A2 shifts the resonant frequencies to 3.8 GHz (3.53–4.16 GHz) and 5.1 GHz (4.7–6.0 GHz), respectively, with corresponding gains of 2.59 dBi and 2.65 dBi.

Measurements have been undertaken across the seven distinct operational modes previously outlined, including the solo modes of A1 (Mode 1) and A2 (Mode 2), and their simultaneous operation (Mode 3). The modes depicted in Fig. 3 are identified as Modes 4 to 7. Fig. 7 shows the antenna’s measured S -parameters. Mode 1 operates at 3.3–3.94 GHz and Mode 2 at 4.28–5.98 GHz. Mode 3 has dual bands: 3.6–4.28 GHz and 4.83–6.16 GHz. Modes 4 to 7 share the same

S -parameters, with an operational band of 3.83–4.92 GHz as shown in Fig. 7(f). The corresponding radiation patterns, measured in an anechoic chamber, are presented in Fig. 8.

4. RECONFIGURABLE

The antenna integrates two sets of dipole arms, capable of accessing a variety of distinct operational bands and radiation patterns based on the feeding strategy. The transition between these modes can be facilitated by loading PIN diodes between the ports. By strategically placing PIN diodes between the appropriate ports, the antenna’s different arms are activated, enabling access to a diverse array of at least 13 operational modes through the modulation of diode conduction states (for example, the PIN loading instance shown in Fig. 1 can achieve a mode where A1 and A2 operate simultaneously).

Mode 8 features the conduction of A1’s left arm alongside both arms of A2; Mode 9 is characterized by A1’s right arm and both arms of A2; Mode 10 sees the upper arm of A2 in con-

TABLE 2. Comparison with other designs.

References	Frequency (GHz)	Size	Reconfigurability
[9]	1.65, 2, 2.4	$0.99 \times 0.99\lambda_0$	Frequency and pattern
[13]	3.54–4.46	$2.36 \times 0.98\lambda_0$	Frequency and pattern
[14]	2.15–2.99	$1.72 \times 0.57\lambda_0$	Frequency and pattern
[15]	1.52–3.2	$0.61 \times 0.2\lambda_0$	Frequency and pattern
This work	Typical resonance: 3.5, 3.8, 4.2, 4.9, 5.1	$0.36 \times 0.35\lambda_0$	Frequency and pattern

junction with both arms of A1; Mode 11 involves the lower arm of A2 with both arms of A1; Mode 12 combines A1's left arm with A2's upper arm and A1's right arm with A2's lower arm; Mode 13 synchronizes A1's left arm with A2's lower arm and A1's right arm with A2's upper arm. A schematic of these six additional operational modes is presented in Table 1, alongside the respective S -parameters and radiation patterns for each.

Beyond the operational modes already discussed, an additional six modes can be achieved by altering the loading method of the diodes, as follows: Mode 8 involves the conduction of A1's left arm and both arms of A2; Mode 9 involves A1's right arm and both arms of A2; Mode 10 involves the upper arm of A2 and both arms of A1; Mode 11 involves the lower arm of A2 and both arms of A1; Mode 12 involves the simultaneous conduction of A1's left arm with A2's upper arm and A1's right arm with A2's lower arm; Mode 13 involves the simultaneous conduction of A1's left arm with A2's lower arm and A1's right arm with A2's upper arm. A schematic of these six additional operational modes is presented in Table 1, alongside the respective S -parameters and radiation patterns for each.

Table 1 indicates that the antenna exhibits distinct resonant frequencies across various operational modes, all characterized by symmetric radiation patterns. Specifically, Modes 8 and 9 demonstrate dual-band resonance at 3.86 GHz and 5.13 GHz. Modes 10 and 11 share a single resonant frequency at 4.83 GHz, and both Modes 12 and 13 resonate at 5.0 GHz. Table 2 compares the proposed antenna against existing designs, revealing its distinct advantages in multi-band functionality and compactness.

5. CONCLUSIONS

The design and development of a reconfigurable, multi-mode antenna featuring a partially excavated cloverleaf structure have been successfully demonstrated. This antenna supports 13 operational modes with different operating bands and radiation patterns, meeting the frequency demands of 5G and forthcoming communication systems. The prototype's measured performance corroborates the simulated results, underscoring its aptness for compact, high-performance wireless applications.

ACKNOWLEDGEMENT

This work was supported by "The Fundamental Research Funds for the Central Universities", Southwest Minzu University (ZYN2024134).

REFERENCES

- [1] Tandel, T. and S. Trapasiya, "Reconfigurable antenna for wireless communication: Recent developments, challenges and future," *Wireless Personal Communications*, Vol. 133, No. 2, 725–768, 2023.
- [2] Subbaraj, S. and S. B. Thomas, "Reconfigurable antennas and their practical applications — A review," *Radio Science*, Vol. 58, No. 9, 1–13, 2023.
- [3] Hussain, Q., D. Choi, N. Hussain, A. Abbas, M. A. Sufian, and N. Kim, "Design and improvement of a wideband angled dipole array antenna for S-band applications," in *2023 17th European Conference on Antennas and Propagation (EuCAP)*, 1–3, Florence, Italy, 2023.
- [4] Joshi, C., A. C. Lepage, J. Sarrazin, and X. Begaud, "Size, gain and bandwidth trade-offs for wideband diamond dipole with AMC reflector," *AIP Conference Proceedings*, Vol. 1715, No. 1, 020051, Mar. 2016.
- [5] Ramahatla, K., M. Mosalaosi, A. Yahya, and B. Basutli, "Multi-band reconfigurable antennas for 5G wireless and CubeSat applications: A review," *IEEE Access*, Vol. 10, 40910–40931, 2022.
- [6] Ali, T., S. Pathan, and R. C. Biradar, "Multiband, frequency reconfigurable, and metamaterial antennas design techniques: Present and future research directions," *Internet Technology Letters*, Vol. 1, No. 6, e19, 2018.
- [7] Ullah, U., M. Al-Hasan, S. Koziel, and I. B. Mabrouk, "EM-driven size reduction and multi-criterial optimization of broadband circularly-polarized antennas using pareto front traversing and design extrapolation," *Scientific Reports*, Vol. 12, No. 1, 9877, 2022.
- [8] Pakkathillam, J. K. and M. Kanagasabai, "Circularly polarized broadband antenna deploying fractal slot geometry," *IEEE Antennas and Wireless Propagation Letters*, Vol. 14, 1286–1289, 2015.
- [9] Jiao, Z. and Y. Zhao, "Design of frequency and beam reconfigurable antenna based on encoded reflectors for Wi-Fi and IoT applications," *AIP Advances*, Vol. 14, No. 6, 065127, 2024.
- [10] Ali, S. A., M. Wajid, A. Kumar, and M. S. Alam, "Design challenges and possible solutions for 5G SIW MIMO and phased array antennas: A review," *IEEE Access*, Vol. 10, 88567–88594, 2022.
- [11] Wang, H., A. Ali, Y. B. Park, and I. Park, "A mode-compressed wideband dipole antenna integrated with solar cell for dual-functional operation," *IEEE Transactions on Antennas and Propagation*, Vol. 71, No. 12, 9932–9937, 2023.
- [12] Takeshore, K., S. Singh, C. Sairam, and S. D. Ahirwar, "Design of asymmetric wideband printed dipole antenna using inset feeding technique," *Progress In Electromagnetics Research C*, Vol. 96, 87–96, 2019.
- [13] You, C. J., S. H. Liu, J. X. Zhang, X. Wang, Q. Y. Li, G. Q. Yin, and Z. G. Wang, "Frequency- and pattern-reconfigurable

- antenna array with broadband tuning and wide scanning angles,” *IEEE Transactions on Antennas and Propagation*, Vol. 71, No. 6, 5398–5403, 2023.
- [14] Hu, J., X. Yang, L. Ge, Z. Guo, Z.-C. Hao, and H. Wong, “A reconfigurable 1×4 circularly polarized patch array antenna with frequency, radiation pattern, and polarization agility,” *IEEE Transactions on Antennas and Propagation*, Vol. 69, No. 8, 5124–5129, 2021.
- [15] Zhang, Y., S. Lin, Z. Yang, B. Li, J. Cui, and J. Jiao, “A pattern- and frequency-reconfigurable antenna using liquid metal,” *Microwave and Optical Technology Letters*, Vol. 63, No. 5, 1499–1506, 2021.